Supplementary Figures for

Bifunctional iRGD-anti-CD3 enhances antitumor potency of T cells by facilitating tumor infiltration and T cell activation

Zhou S, *et al. J Immunother Cancer* 2021; 9:e001925. doi: 10.1136/jitc-2020-001925

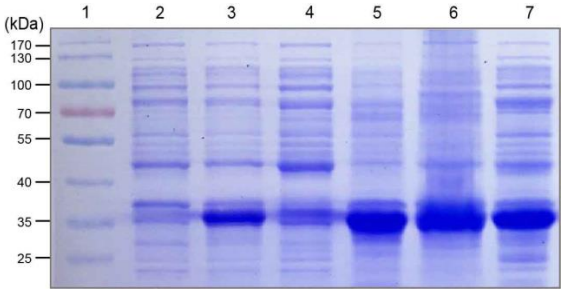

Fig. S1: SDS-PAGE analysis of iRGD-anti-CD3 expression. Lane 1, protein ladder; Lane 2, bacteria without IPTG induction; Lane 3, bacteria induced with 1 mM IPTG; Lane 4, the supernatant of the ultrasonic lysate; Lane 5, the precipitation of the ultrasonic lysate; Lane 6, solubilized inclusion bodies; Lane 7, Refolded products.

Zhou S, *et al. J Immunother Cancer* 2021; 9:e001925. doi: 10.1136/jitc-2020-001925

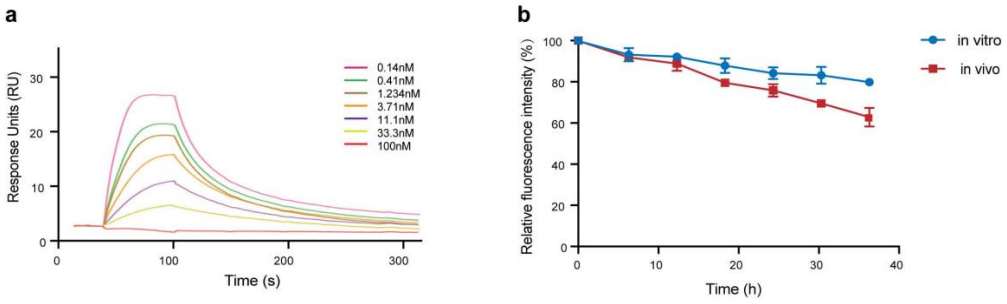

Fig. S2: (a) Binding kinetics of iRGD-anti-CD3 by SPR measurements and traces are shown at indicated concentrations. **(b)** Changes in overall fluorescence intensities of iRGD-anti-CD3 both on cell surface and in the cytoplasm of modified T cells.

Zhou S, *et al. J Immunother Cancer* 2021; 9:e001925. doi: 10.1136/jitc-2020-001925

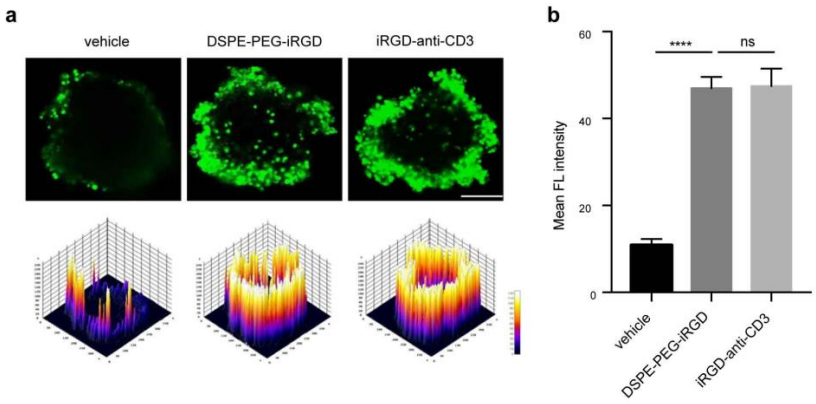

Fig. S3: Comparison of iRGD-anti-CD3 with DSPE-PEG-iRGD in promoting T cell penetration in MCSs. **(a)** PBMCs modified with iRGD-anti-CD3 or T cells modified with DSPE-PEG-iRGD were added into the MCSs at an E:T ratio of 5:1. After incubation for 24 h at 37 °C, confocal images and surface plot images were acquired. scale bar, 100 μm. **(b)** Mean fluorescence intensity of T cells in MCSs. Data are analyzed with Student's t test unless specified, and represented as mean ± SEM. ns, not significant; ***p < 0.001.

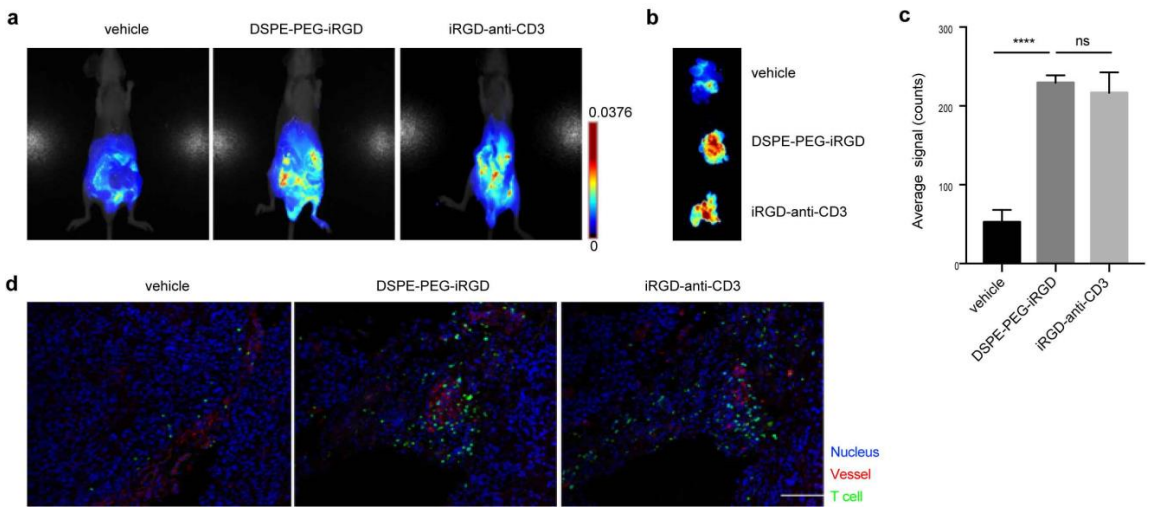

Fig. S4: Comparison of iRGD-anti-CD3 with DSPE-PEG-iRGD in promoting T cell penetration in MKN45 peritoneal metastatic mouse model. (a) 1×10^7 T cells modified in two approaches were injected intraperitoneally into MKN45 tumor-bearing mice. The mice and **(b)** tumor nodules were scanned 6 h post injection. **(c)** Semiquantification of T cell signal in tumor nodules from (b). **(d)** Immunofluorescence analysis of tumor sections. scale bar, 100 μm. Data are analyzed with Student's t test unless specified, and represented as mean ± SEM. ns, not significant; ***p < 0.001.

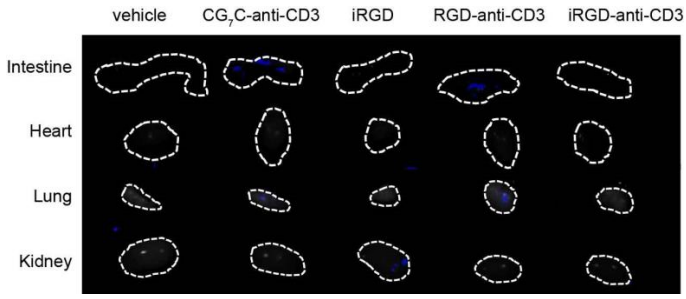

Fig. S5：T cell signal of normal organs in the intraperitoneal tumor model. *Ex vivo* images of other normal organs including intestine, heart, lung, kidney at 6 h post injection. White dotted lines showed where the organs were placed.

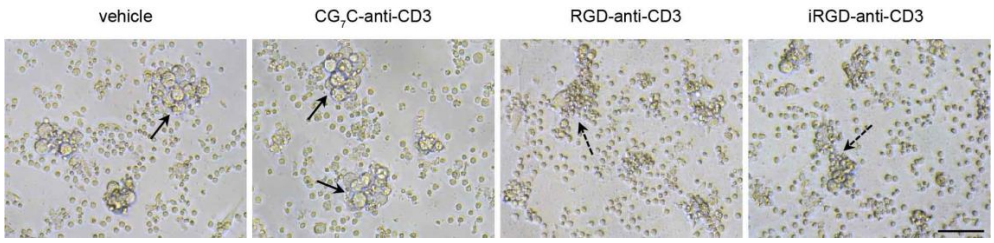

Fig. S6: iRGD-anti-CD3 modification enhanced T cell cytotoxicity against MKN45 cells. Light microscopy of monolayer tumor cell cultures after incubation with modified PBMCs at an E/T of 20:1 for 24h. Solid arrows, surviving tumor cell clumps; dotted arrows, lysed tumor cells. Scale bar, 100 μm.

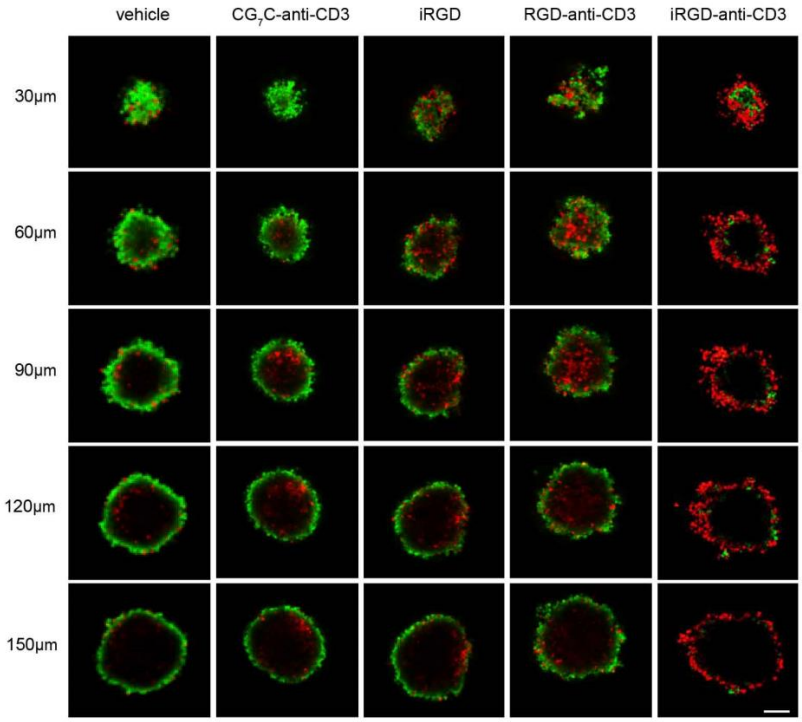

Fig. S7: iRGD-anti-CD3 improved T cell cytotoxicity against HGC27 spheroids.

Consecutive confocal images showing live/dead cells in MCSs with 30 μm intervals. Magnification, ×200; Scale bar, 100 μm.

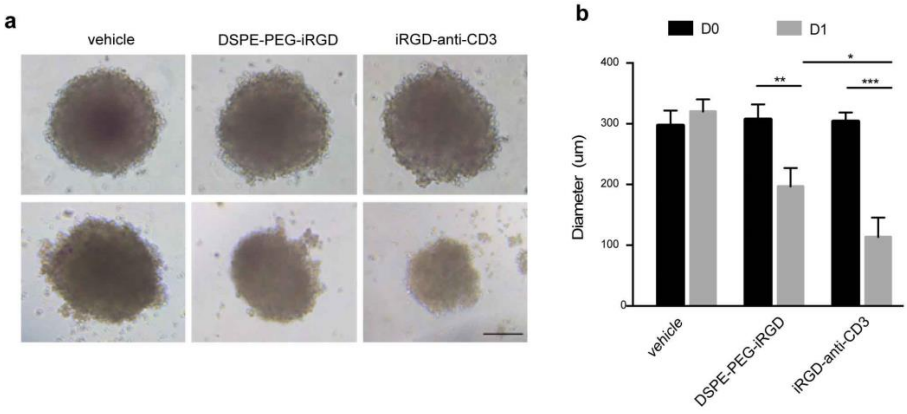

Fig. S8: Antitumor effect of T cells modified with iRGD-anti-CD3 or DSPE-PEG-iRGD in MCSs. (a) modified PBMCs or T cells were added into the MCSs at an E:T ratio of 20:1. Light microscopy of spheroids were acquired at 24 h. scale bar, 100 μm. **(b)** Diameter comparison of MCSs. Data are analyzed with Student's t test unless specified, and represented as mean ± SEM. ns, not significant; **$p < 0.01$; ***$p < 0.001$.

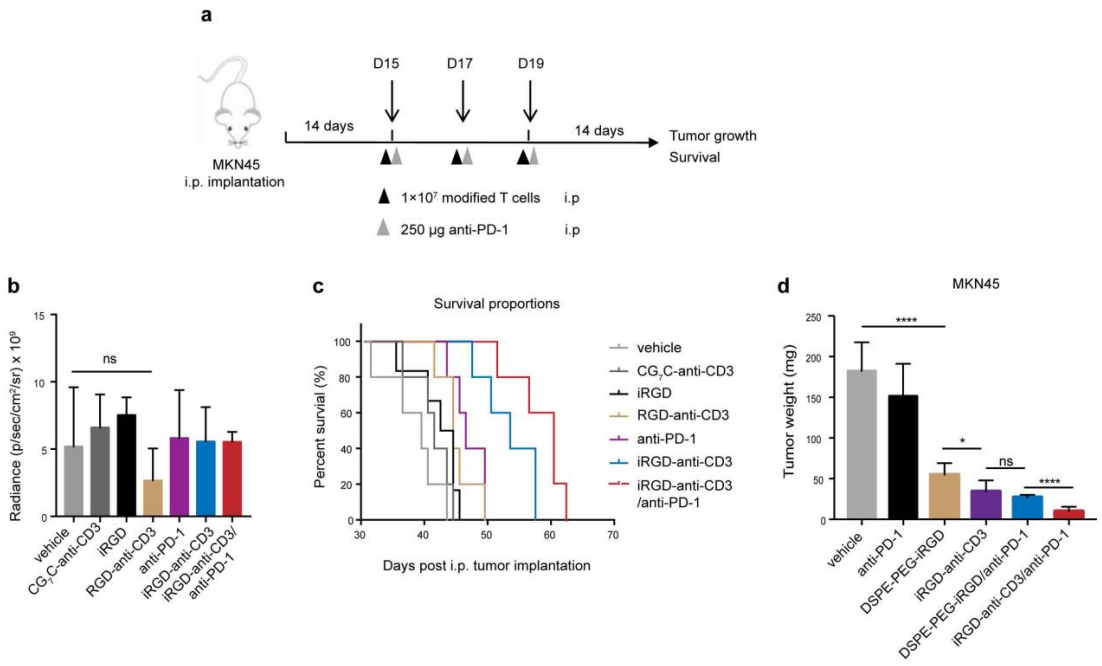

Fig. S9: Combining iRGD-anti-CD3-modified T cells with PD-1 blockade in MKN45 peritoneal metastatic mouse model. **(a)** Schematic illustration of treatment process in peritoneal metastasis mouse models. **(b)** Baseline tumor burden before the treatment started (at day 14). **(c)** Survival analysis of all treatment groups. **(d)** Mice bearing disseminated MKN45 peritoneal tumors received intraperitoneal injection of 1×10^7 T cells modified in two approaches every other day for 3 times. 250 μg PD-1 blockade was given intraperitoneally every other day for 3 injections. Tumors were harvested after 2 weeks of treatment and weighed. Data are analyzed with Student's t test unless specified, and represented as mean ± SEM. ns, not significant; *$p < 0.05$; ****$p < 0.0001$.

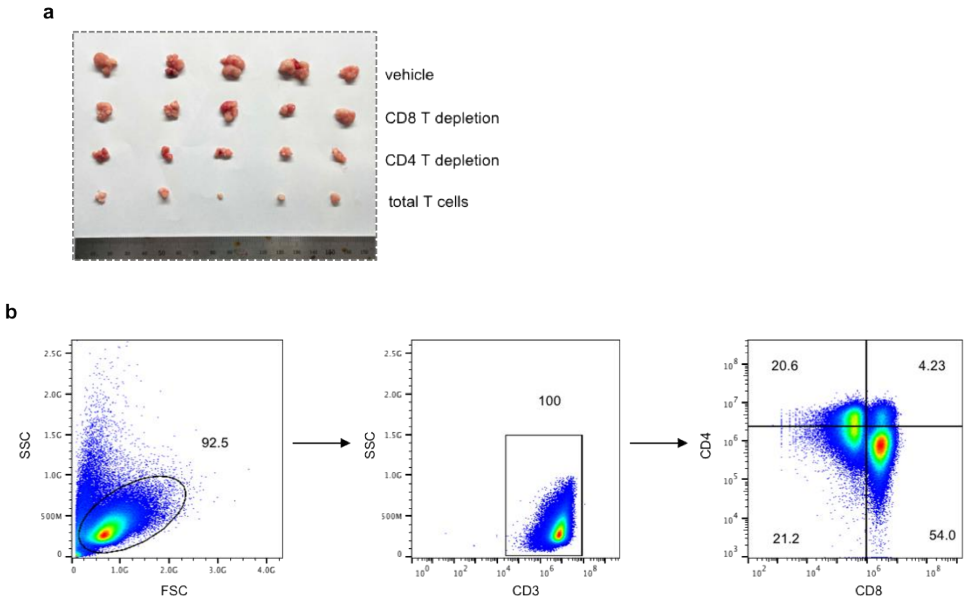

Fig. S10: **(a)** Tumor nodules in Fig. 4g were photographed. **(b)** Representative sequential gating strategies for negative isolation of $CD3^+CD4^+$ and $CD3^+CD8^+$ T cells.

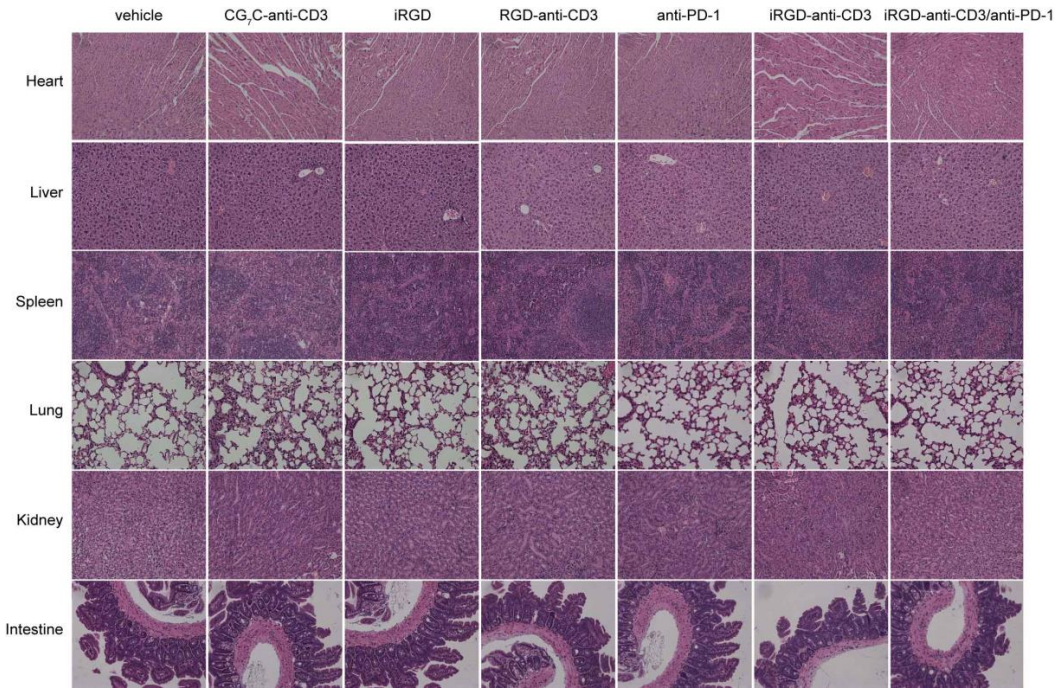

Fig. S11: H&E staining of major organs in MKN45 peritoneal metastatic mouse model. organs in all groups were harvested and stained with H&E at 28 days post tumor implantation.

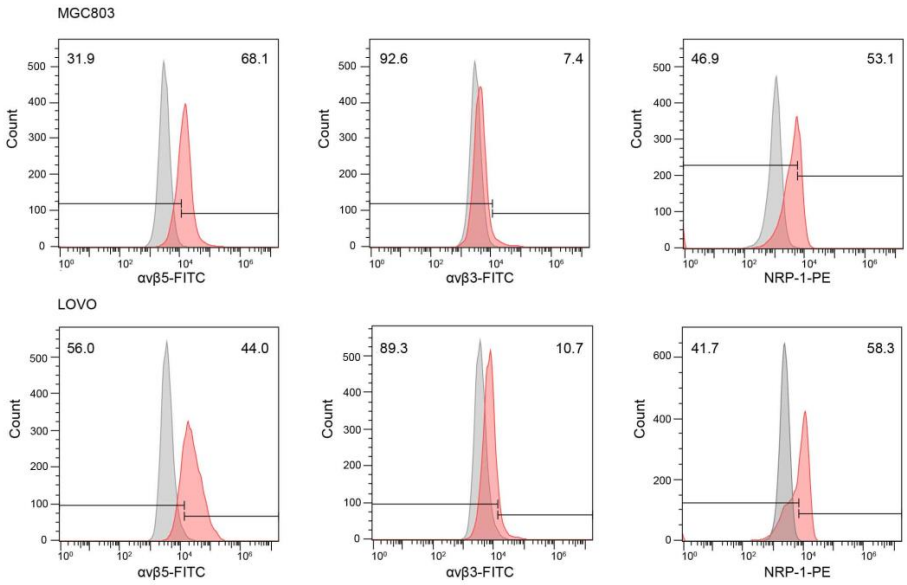

Fig. S12: Expression of αvβ5, αvβ3, and NRP-1 on MGC803 and LOVO cells. Integrin αvβ5 was detected using FITC-conjugated mouse anti-human αvβ5 monoclonal antibody, and integrin αvβ3 was detected using FITC-conjugated mouse anti-human αvβ3 monoclonal antibody. The matched isotype control was FITC-conjugated mouse IgG1κ. NRP-1 was detected using PE-conjugated mouse anti-human NRP-1 monoclonal antibody and an isotype control.

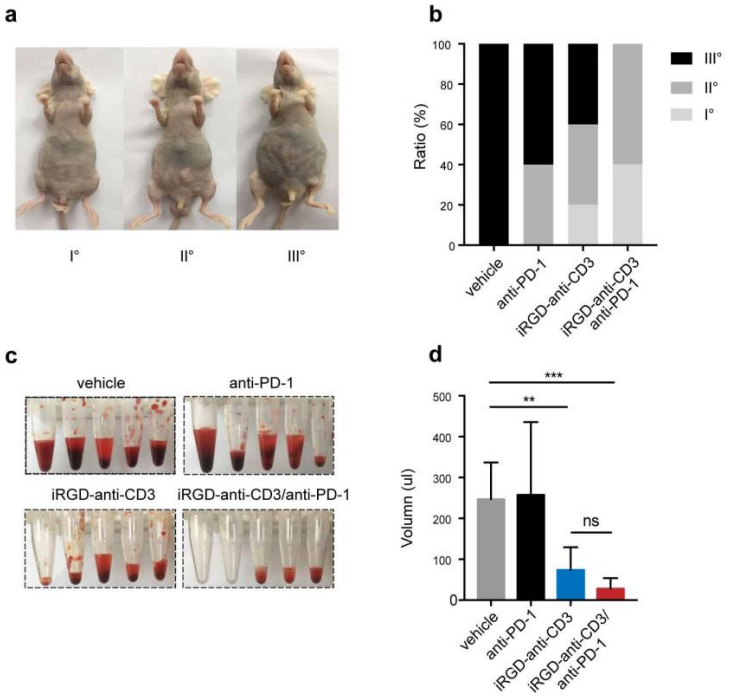

Fig. S13: Combination of iRGD-anti-CD3-modified T cells with PD-1 blockade showed potent tumor inhibition in LOVO peritoneal metastatic colon cancer model. (a) Grading standard of abdominal distention: grade I, invisible distension of abdomen; grade II, moderate symmetrical distension of abdomen; grade III, marked abdominal distention with massive ascites. **(b)** Comparison of abdomen distension in all groups. **(c)** Images of ascites collected in Eppendorf tubes and **(d)** ascites volumes were compared. Data are analyzed with Student's t test unless specified, and represented as mean ± SEM. ns, not significant; *p < 0.05; **p < 0.01; ***p < 0.001.

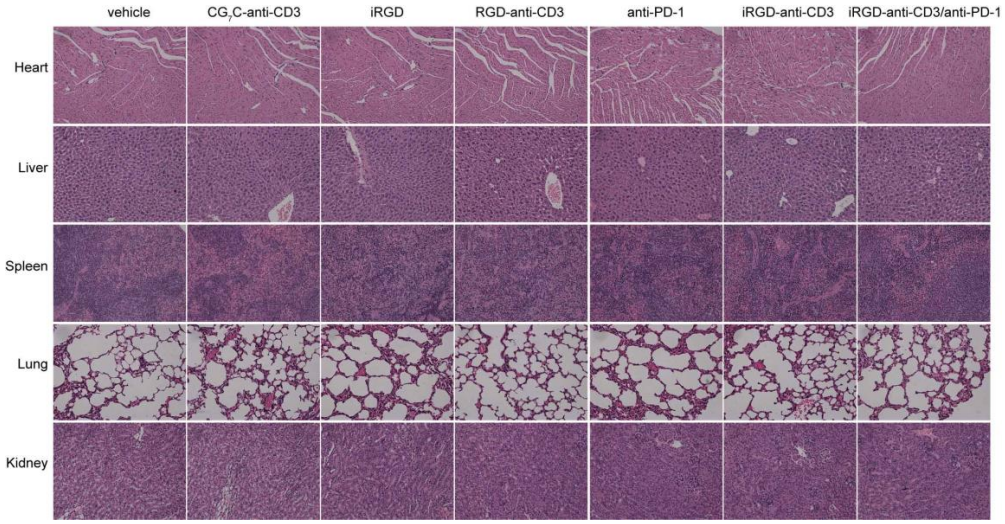

Fig. S14: H&E staining of major organs in MKN45 subcutaneous mouse model. organs in all groups were harvested and stained with H&E at 25 days post tumor implantation.